Journal of Power Sources 236 (2013) 80–86

Contents lists available at SciVerse ScienceDirect

Journal of Power Sources

journal homepage: www.elsevier.com/locate/jpowsour

Study on microstructure and electrochemical performance of the $MlNi_{3.55}Co_{0.75-x}Mn_{0.4}Al_{0.3}(Cu_{0.75}P_{0.25})_x$ ($x = 0$–0.5) composite alloys

Bo Zhang, Wenyuan Wu*, Xue Bian, Ganfeng Tu

Institute of Materials and Metallurgy, Northeastern University, Shenyang 110000, PR China

HIGHLIGHTS

- All the alloy electrodes exhibit favorable activation properties.
- The cycle stability is improved due to the multiple substitution.
- The high-rate discharge capability is improved especially at high discharge current.
- The charge-transfer resistance decreases and the exchange current density increases.
- The hydrogen diffusion coefficient increases with increasing Cu–P content.

ARTICLE INFO

Article history:
Received 7 September 2012
Received in revised form
12 February 2013
Accepted 14 February 2013
Available online 26 February 2013

Keywords:
Hydrogen absorbing materials
Microstructure characteristics
Electrochemical properties
Kinetics properties

ABSTRACT

In order to improve the high-rate discharge capability without diminishing the cycle stability, we investigate the substitution of Cu–P for Co on the microstructure and electrochemical properties of the $MlNi_{3.55}Co_{0.75-x}Mn_{0.4}Al_{0.3}(Cu_{0.75}P_{0.25})_x$ ($x = 0$–0.5) composite alloys. The results obtained by XRD, SEM and EDS show that the $MlNi_{3.55}Co_{0.75}Mn_{0.4}Al_{0.3}$ alloy consists of a single phase, and the substitutional alloys are composed of multiphase structures. The electrochemical studies reveal that the substitutional alloys can be easily activated within one cycle, but the maximum discharge capacity decreases from 296.8 mA h g^{-1} ($x = 0$) to 275 mA h g^{-1} ($x = 0.5$). With the increase of Cu–P content, the capacity decay rate D_{100} initially decreases from 1.26 mA h g^{-1} $cycle^{-1}$ ($x = 0$) to 0.80 mA h g^{-1} $cycle^{-1}$ ($x = 0.3$), and then increases to 1.19 mA h g^{-1} $cycle^{-1}$ ($x = 0.5$). The overall high-rate discharge capability is significantly improved with increasing Cu–P content, which is in agreement with the monotonous increase of the exchange current density and the hydrogen diffusion coefficient. The best compromise between excellent high-rate discharge capacity and favorable cycle stability of the series alloys is obtained when $x = 0.3$.

1. Introduction

In recent years, the secondary battery with favorable rate discharge capability and long cycle life is urgently demanded as a power source for hydride electric vehicles and electric automobiles. The MH/Ni battery is one of the most promising candidates in dynamic power fields [1–4]. However, some disadvantages based on the commercial AB_5-type hydrogen storage alloys have restricted their widespread applications. In order to overcome these drawbacks and improve the overall electrochemical properties, many efforts have been made [5–9]. Up to now, element substitution has been one of the most effective methods to provide optimum performance for the MH/Ni batteries.

The AB_5-type hydrogen storage alloy $MlNi_{3.55}Co_{0.75}Mn_{0.4}Al_{0.3}$ is now extensively used in commercial batteries. It is confirmed in the literature [10–13] that Co remarkably decreases the lattice expansion during the hydrogen absorbing/desorbing processes, and therefore plays a crucial role in the cycle stability for the composite alloys. However, in addition to account for 50% of the total cost of the raw material, Co has an adverse effect on the high-rate discharge performance. Pan et al. [14] indicated that the substitution of Co for Ni in $MlNi_{4.3-x}Co_xAl_{0.7}$ ($x = 0$, 0.3, 0.5, 0.7, 0.9, 1.1, and 1.3) alloys caused the exchange current density to decrease from 395 to 33 mA g^{-1}, the limiting current density to decrease from 2263 to 308 mA g^{-1}, the hydrogen diffusion coefficient to decrease from 1.42×10^{-10} to 2.1×10^{-11} cm^2 s^{-1} respectively. With this view in mind, the reduction of cobalt in hydrogen storage alloys would be a significative task. In the present work, it is often investigated by means of partial or total replacement of cobalt by other

* Corresponding author. Tel./fax: +86 (0)24 83680527.
E-mail address: WuWY8368@hotmail.com (W. Wu).

0378-7753/$ – see front matter © 2013 Elsevier B.V. All rights reserved.
http://dx.doi.org/10.1016/j.jpowsour.2013.02.052

transitional elements. Nevertheless, various $LaNi_5$-type alloys with the low-Co content show inferior cycle life as the function of Co on the cycle stability is extremely important. Therefore, we adopt Cu–P additives as the substitutional element. Firstly, Cu possesses superior electrical conductivity and smaller interaction with hydrogen atoms, which is in favor of the kinetics properties of the hydrogen storage alloys. Secondly, P possesses favorable corrosion resistance, which is normally used as the surface coating and plating for hydrogen storage alloys in the previous investigations. In addition, the multiphase structure is in favor of the hydrogen diffusion behavior, because the phase boundaries can act as fast diffusion paths for hydrogen absorption.

We have studied the kinetics properties of the Cu–P containing alloys by the electrochemical impedance spectroscopy method in our previous investigations [15]. The results indicated that the kinetics properties of the substitutional alloys were improved. For further research, we investigated the influence of the substitution of Cu–P for Co on the microstructure and electrochemical performance of the composite alloys $MlNi_{3.55}Co_{0.75-x}Mn_{0.4}Al_{0.3}(Cu_{0.75}P_{0.25})_x$ ($x = 0$–0.5) in this paper. The purpose of this work is to improve the high-rate discharge capability without diminishing the cycle life.

2. Experimental details

2.1. Alloy preparation

The nominal composition of the investigated alloys was $MlNi_{3.55}Co_{0.75-x}Mn_{0.4}Al_{0.3}(Cu_{0.75}P_{0.25})_x$ ($x = 0$–0.5), where Ml denoted La-rich mixed mischmetal composed of 55.95% La, 30.77% Ce, 4.23% Pr, 9.05% Nd (mass fraction). The experimental alloys were prepared in an intermediate frequency induction furnace under argon atmosphere with a pressure of 0.4 MPa and cooled in a water-cooling copper crucible. A slight excess Ml, Al was used to compensate for evaporative loss during the melting. Then, 5 kg alloy ingots were obtained and some of them were mechanically crushed into alloy powders, which were captured between sieves of 400 mesh size for X-ray diffraction (XRD) measurements and 300 mesh size for electrochemical analysis.

2.2. Electrode preparation and electrochemical measurement

The test electrodes were prepared by cold-pressing a mixture of 0.1 g alloy powders and 0.3 g nickel powders (T255) into a pellet of 10 mm in diameter under 10 MPa. The electrochemical measurements were tested by a tri-electrode open cell, consisting of a metal hydride electrode, a sintered $NiOOH/Ni(OH)_2$ counter electrode and a Hg/HgO reference electrode. The electrolyte was 6 M KOH aqueous solution. In order to reduce the ohmic drop between the working electrode and the reference electrode, a Luggin capillary was located close to the hydride electrode. The electrodes were fully charged at 100 mA g^{-1} and discharged at 100 mA g^{-1} in the electrochemical measurements. The discharge cut-off potential was set at −0.6 V vs. Hg/HgO reference electrode. The high-rate discharge capacity is defined as $HRD = (C_d/(C_d + C_{100})) \times 100\%$, where C_d is the discharge capacity of the electrode at the current density $I_d = 300, 600, 900, 1200, 1500$ mA g^{-1}, C_{100} is the residual discharge capacity measured at the current density of 100 mA g^{-1}. The cycle stability examination is determined by the following equation: $D_{100} = (C_{max} - C_{100})/(100 - n)$, where D_{100} is the capacity decay rate in 100 cycles, C_{max} is the maximum discharge capacity, C_{100} is the discharge capacity after 100 cycles, n is the activation number.

The electrochemical measurements were carried out by Autolab PGSTAT30 electrochemical workstation at 50% depth of discharge (DOD). The linear polarization curves of the electrodes were measured by scanning the electrode potential at the rate of 0.1 mV s^{-1} from −10 to 10 mV (vs. open-circuit potential).

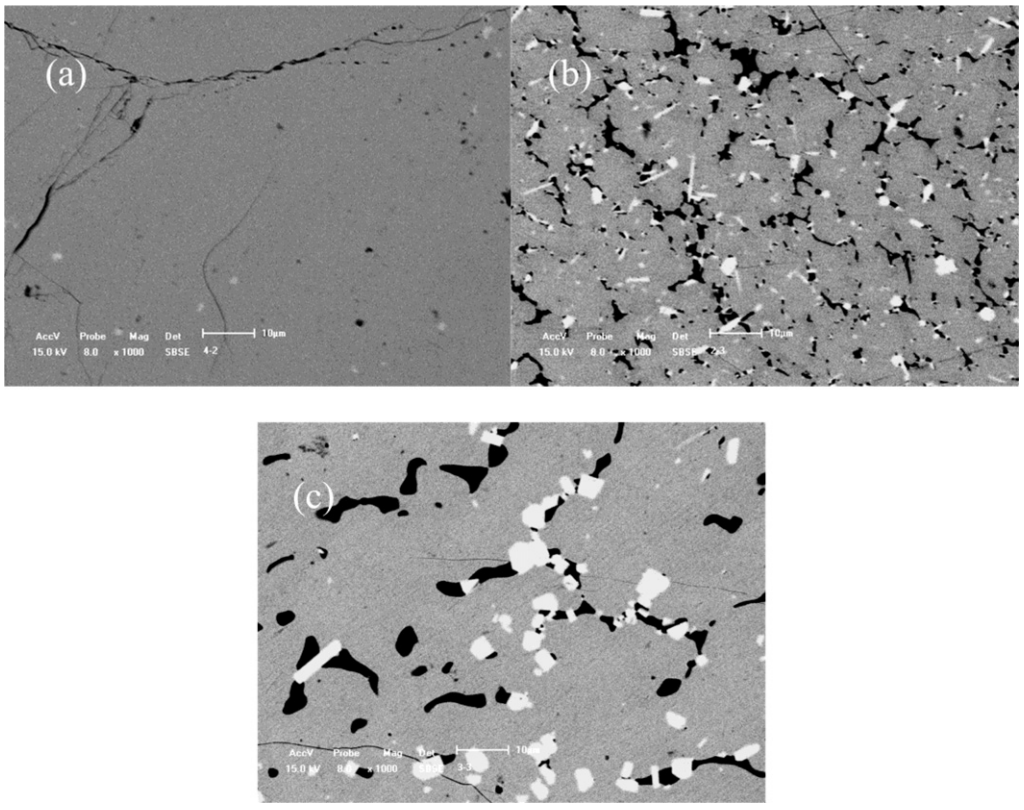

Fig. 1. SEM backscattering electron images of the $MlNi_{3.55}Co_{0.75-x}Mn_{0.4}Al_{0.3}(Cu_{0.75}P_{0.25})_x$ alloys: (a) $x = 0$; (b) $x = 0.3$; (c) $x = 0.5$.

Table 1
Chemical compositions of the three phases for $MlNi_{3.55}Co_{0.25}Mn_{0.4}Al_{0.3}(Cu_{0.75}P_{0.25})_{0.5}$ alloy using EDS (unit: at.%).

Phases	La	Ce	Pr	Nd	Ni	Co	Cu	Mn	Al	P
Matrix phase	9.21	5.62	1.15	1.89	63.8	2.62	6.03	4.05	5.68	–
White phase	21.3	6.44	–	1.95	32.9	–	1.67	–	–	35.8
Black phase	2.93	1.40	–	–	48.5	2.73	2.37	23.2	17.6	1.24

For galvanostatic intermittent titration technique (GITT) measurement, a small current 30 mA was applied to the electrode for a short time of 20 s, and then the current varied to 0 mA and lasted few seconds.

2.3. Microstructure determination and morphology observation

A Shimadzu SSX-550 scanning electron microscopy was used for morphological characterization of the investigated alloys. An Inspect F-50 scanning electron microscopy linked with an X-Max energy dispersive spectrometer was used for chemical analysis of the investigated alloys. XRD data were collected by step-scanning method using a PANalytical X' Pert Pro X-ray diffractometer with Cu Kα radiation. The 2θ range of the samples was from 10° to 90°, with a step interval of 0.02° and a count time of 2° min^{-1}. For the corrosion experiments, the samples of the alloys were etched with corrosive solution, which consisted of 70% nitric acid, 5% HF and 25% deionized water (volume ratio).

3. Results and discussion

3.1. Microstructure measurements

It is observed that the $MlNi_{3.55}Co_{0.75}Mn_{0.4}Al_{0.3}$ alloy consists of a single phase as shown in Fig. 1(a), and the white spot is ascribed to the impurities of the crucible. The substitutional alloys differ both chemically and structurally from the base alloy, which are composed of three phases as shown in Fig. 1(b) and (c), the white phase (white area), the black phase (black area) and the matrix phase (light gray area). The chemical compositions of the three phases of $x = 0.5$ alloy were measured by EDS, and the results are listed in Table 1.

The EDS analysis shows that the white phase in the $MlNi_{3.55-}Co_{0.25}Mn_{0.4}Al_{0.3}(Cu_{0.75}P_{0.25})_{0.5}$ alloy, which corresponds to the white area in Fig. 1 is predominantly rich P with a higher Ml percentage than the matrix phase (light gray area) as shown in Table 1. For the matrix phase, the element ratio is 1:5 for RE: (Ni Co Mn Al), which validates the matrix is $LaNi_5$-type structure. The black phase with larger amounts of Mn as shown in Fig. 1 precipitates dispersively in the main phase. This is reasonable because the formation of white phase captures the Ml and Ni elements from the main phase, thus leading to a deviation from stoichiometry and the transitional elements form precipitated phase. The backscattered electron images demonstrate that element Cu mainly distributes in the matrix phase as shown in Fig. 2(b). In addition, P and Mn both precipitate in the alloys which is correspondence to the results of EDS. In combination with Fig. 1, the morphologies and distributions

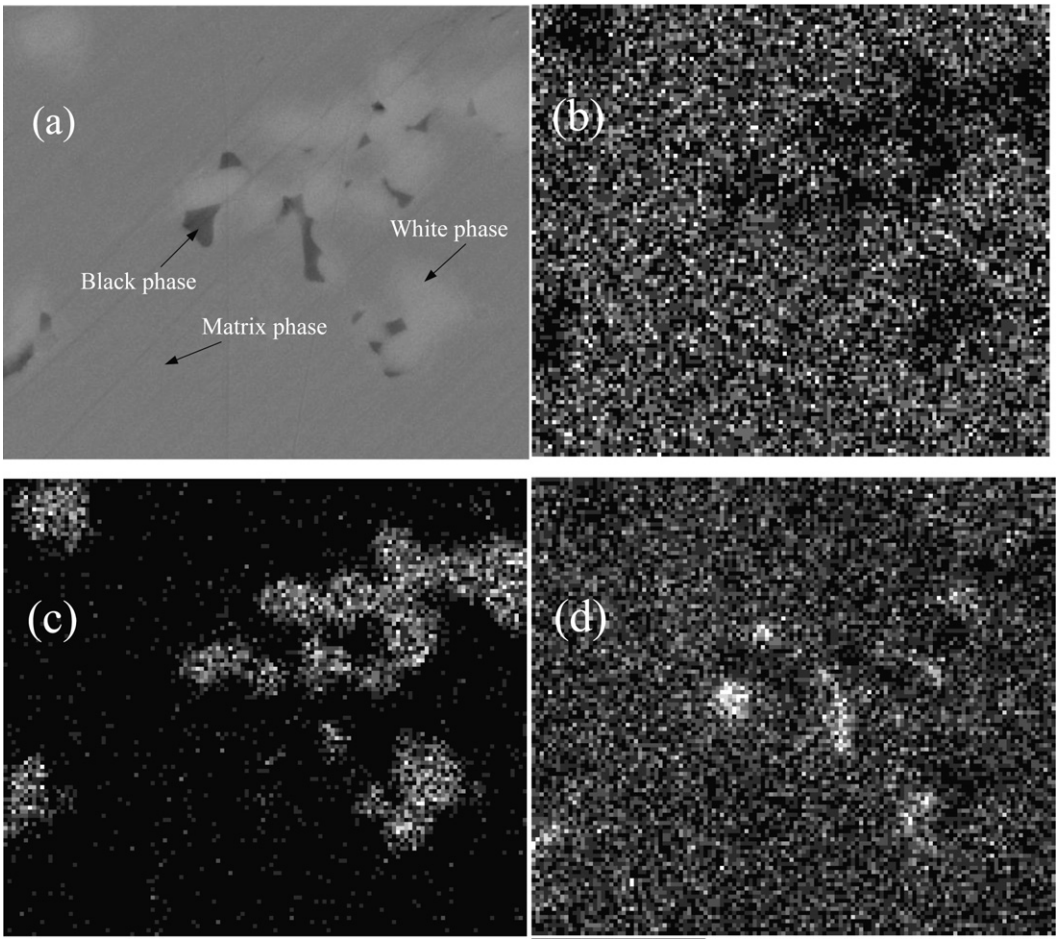

Fig. 2. SEM backscattering electron image (a) and EDS elemental mappings of Cu (b), P (c), Mn (d) for the $MlNi_{3.55}Co_{0.25}Mn_{0.4}Al_{0.3}(Cu_{0.75}P_{0.25})_{0.5}$ alloy.

of the three phases vary with the increase of Cu–P content. It can be seen that the strip-like white phase and black phase embed in the matrix for the alloys of $x = 0.3$, whereas the two phases appear block-shape for the alloy of $x = 0.5$.

The XRD patterns of the $MlNi_{3.55}Co_{0.75-x}Mn_{0.4}Al_{0.3}(Cu_{0.75}P_{0.25})_x$ ($x = 0$–0.5) alloys are illustrated in Fig. 3(a). It is observed that the $MlNi_{3.55}Co_{0.75}Mn_{0.4}Al_{0.3}$ alloy exhibits a single phase, while the partial substitutional alloys consist of multiphase structures. The main phase of the series alloys is $LaNi_5$ phase with hexagonal $CaCu_5$ structure. The substitution of Cu–P for Co generates two new diffraction peaks in the low-angle of the XRD patterns as shown in Fig. 3(b). The new peaks are characterized of the second phase, which are composed of P-rich phase and Mn-rich phase. However, as the limited quantity, it is hard to identify the structure of the second phase.

Moreover, it can be derived from Fig. 3(b) that the intensity of the new peaks increases with increasing x, suggesting that the growth of the Cu–P content leads to an increase of the abundance of the second phase. And it should be emphasized that the second phase plays an important role on the electrochemical properties.

3.2. Activation properties

The cycle number dependence of the discharge capacities of the $MlNi_{3.55}Co_{0.75-x}Mn_{0.4}Al_{0.3}(Cu_{0.75}P_{0.25})_x$ ($x = 0$–0.5) alloy electrodes is illustrated in Fig. 4. It can be seen that the maximum discharge capacity decreases from 296.8 mA h g^{-1} ($x = 0$) to 275 mA h g^{-1} ($x = 0.5$). The loss of the electrochemical capacity is mainly ascribed to the multiphase structures, which occupy a bit hydride-forming elements and may not possess reversibly absorbing/desorbing ability. All alloys exhibit favorable activation properties, and the substitutional alloys only need one cycle to achieve the maximum discharge capacity. Although the precipitated phases do not absorb hydrogen, the interfaces and cracks formed around them are helpful to the diffusion performance of hydrogen atoms, thus improving the activation properties [16,17].

3.3. Cycle stability

The Cu–P content dependence on the capacity decay rates of the investigated $MlNi_{3.55}Co_{0.75-x}Mn_{0.4}Al_{0.3}(Cu_{0.75}P_{0.25})_x$ ($x = 0$–0.5) alloys is illustrated in Fig. 5. According to the above mentioned definitions of the capacity decay rate, it can be known that the smaller the capacity decay rate (D), the better the cycle stability of the alloy.

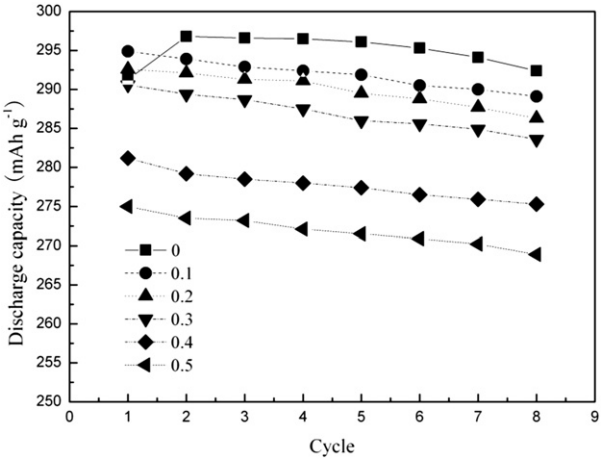

Fig. 4. Activation properties of the $MlNi_{3.55}Co_{0.75-x}Mn_{0.4}Al_{0.3}(Cu_{0.75}P_{0.25})_x$ ($x = 0$–0.5) alloy electrodes.

The relationship between the cycle stability and the amount of Cu–P additives is complex. With the increase of Cu–P content, the values of D_{100} firstly decrease from 1.26 mA h g^{-1} $cycle^{-1}$ ($x = 0$) to 0.80 mA h g^{-1} $cycle^{-1}$ ($x = 0.3$), and then increase to 1.19 mA h g^{-1} $cycle^{-1}$ ($x = 0.5$).

The battery gradually loses efficacy during charging/discharging cycles, and the pulverization is considered to be mainly responsible for the capacity degradation of the hydrogen storage alloys. Actually, the lattice internal stress is the real driving force that leads to the pulverization of the alloy [18,19]. For the $LaNi_5$ metal hydride system, the lattice volume increases by more than 20% in the transition from the solid solution to the full-hydride $LaNi_5H_6$ [20,21]. And the lattice stress inevitably increases when hydrogen atoms enter the crystal framework. On the other hand, the internal stress which is generated by the lattice defects such as the phase boundary, also has a negative influence on the cycle stability of the alloy electrodes. The pulverization leads to micro-cracking and splitting of alloy particles, thus the hydride-forming elements are exposed directly to the alkaline electrolyte and then easily oxidized, which results in the capacity degradation.

The substitution of Cu–P for Co engenders a positive effect on the cycle stability, but cases a contrast tendency when $x > 0.3$. The influence of the Cu–P additives on the cycle stability of the series alloys

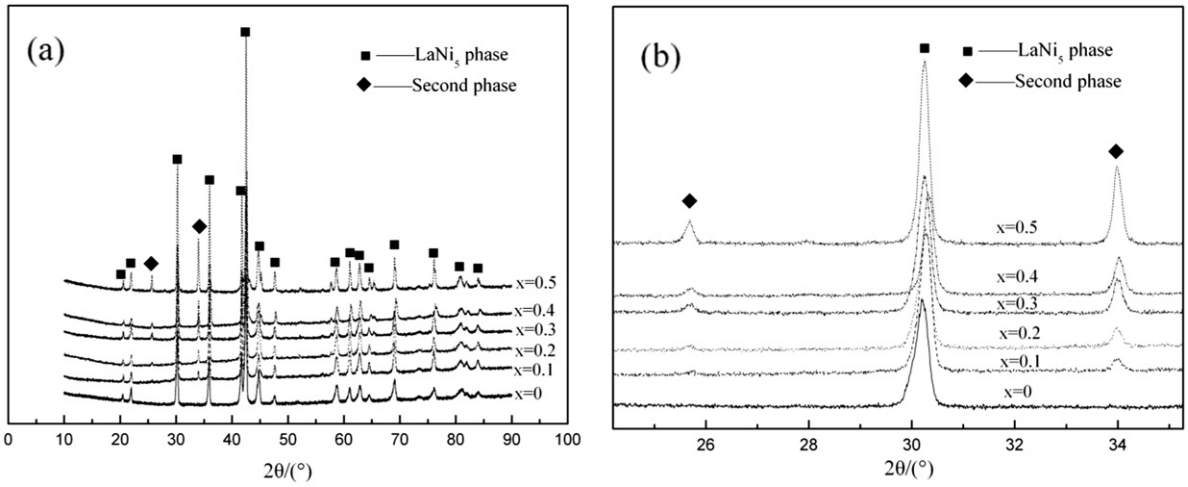

Fig. 3. (a) XRD patterns of the $MlNi_{3.55}Co_{0.75-x}Mn_{0.4}Al_{0.3}(Cu_{0.75}P_{0.25})_x$ ($x = 0$–0.5) alloys; (b) the details in the low-angle range of the XRD patterns.

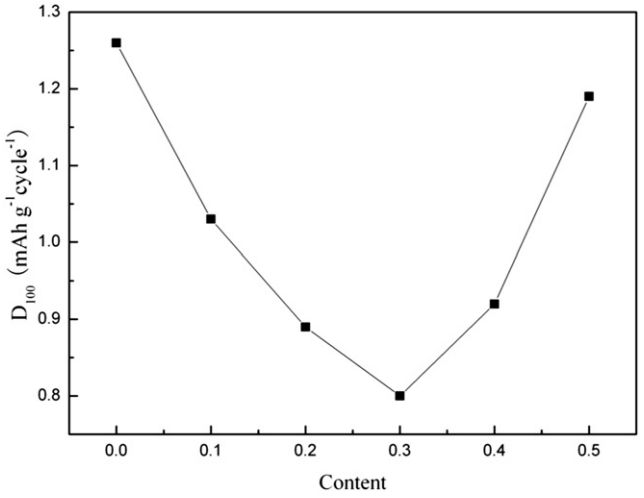

Fig. 5. Capacity decay rate of the $MlNi_{3.55}Co_{0.75-x}Mn_{0.4}Al_{0.3}(Cu_{0.75}P_{0.25})_x$ ($x = 0$–0.5) alloy electrodes.

could be explained by taking into account the following factors. (1) As a non-forming hydride element, Percheron-Guegan et al. [22] indicated that Cu behaved in a similar way to Co on the cycle stability, and the substitution of Cu lowered the Vickers hardness. Notten et al. [23,24] reported that the Cu-containing $La(Ni/Cu)_x$ ($5.0 \leq x \leq 6.0$) alloys provided a larger improvement on the electrochemical cycle stability. It can be concluded that the Cu additive plays the function of Co and is in favor of the cycle stability for the hydrogen storage alloy, but the excess amounts of Cu would decrease the cycle life endurance, because the effects of Cu on the cycle performance are worse than Co. Tang et al. [21] indicated that for the $MlNi_{3.5}Co_{0.7-7x}Cu_{8x}Al_{0.8-x}$ alloy system, about 50% substitution of Cu for Co did not deteriorate the long-term stability, but too much Cu substitution would result in a decrease in the cycle stability.

(2) The most important factor, we suggest that the substitutional alloys contain multiphase structures as shown in Fig. 6. The SEM imagines after corrosion reveal that the sample of the $MlNi_{3.55}Co_{0.75}Mn_{0.4}Al_{0.3}$ alloy is found to be single phase, while the substitutional alloys are composed of two phases, namely $LaNi_5$ phase and P-rich phase, whereas the Mn-rich phase has almost disappeared due to the corrosion. It is apparent that the P-rich phase (white area) separates out on the phase boundary of the matrix phase (deep gray area), which forms a three-dimensional network and serves the function of microencapsulating the main phase grain (deep gray area). Therefore, the P-rich phase in the substitutional alloys plays an important role in suppressing the degeneration during repeating charging/discharging cycles. On the other hand, the lattice defects such as the new phase boundary in the substitutional alloys would increase the lattice internal stress. Since the amounts of the P-rich phase increase with increasing x as shown in Figs. 1 and 3, the excess additives would cause the alloy eager to pulverization and the cycle stability becomes worse. As a result, the influence of the Cu–P content on the cycle stability seems to be a synergistic effect of the alloy microstructure and the substitutional elements, and the series alloys achieve the best cycle stability of the alloy $x = 0.3$.

3.4. Rate discharge capability

The HRD values of the $MlNi_{3.55}Co_{0.75-x}Mn_{0.4}Al_{0.3}(Cu_{0.75}P_{0.25})_x$ ($x = 0$–0.5) alloys as a function of the Cu–P content are exhibited in Fig. 7. It can be seen that the high-rate discharge capability is significantly improved with the increase of Cu–P content. At the high discharge current density 1500 mA g^{-1}, the values of HRD increase from 48.23% to 67%.

High-rate discharge ability of MH/Ni batteries is determined by the kinetics properties of corresponding hydrogen absorbing/desorbing reactions [25,26], and is the key factor to evaluate whether the battery can be used as the power source in the electric vehicles. The kinetics performance basically depends on the resistance of charge-transfer at the electrode surface and the diffusion rate of hydrogen atoms within the bulk alloy, which can be expressed as the exchange current density (I_0) and the hydrogen diffusion coefficient (D) respectively [27–29]. All the kinetics parameters are related to the composition and the microstructure of the hydrogen storage alloys.

The exchange current density (I_0) for the hydride electrode reaction which is used to characterize the electrocatalytic activity for charge-transfer at the metal/electrolyte interface can be obtained by the following formula [30]:

$$I_0 = \frac{IRT}{F\eta} \tag{1}$$

where R_{ct} is the charge transfer resistance, I is the applied current density, R is the gas constant, T is the absolute temperature, F is the Faraday constant and η is the over-potential of the electrochemical reaction for the hydrogen storage alloy. The linear polarization curves as shown in Fig. 8 and the values of R_{ct} and I_0 of the investigated alloy electrodes are listed in Table 2.

It is found that R_{ct} decreases from 421.9 mΩ ($x = 0$) to 173.4 mΩ ($x = 0.5$) and I_0 increases from 61.88 mA g^{-1} ($x = 0$) to 150.5 mA g^{-1} ($x = 0.5$), which proves that the electrocatalytic activity for the charge-transfer process is improved as the substitution. The reason

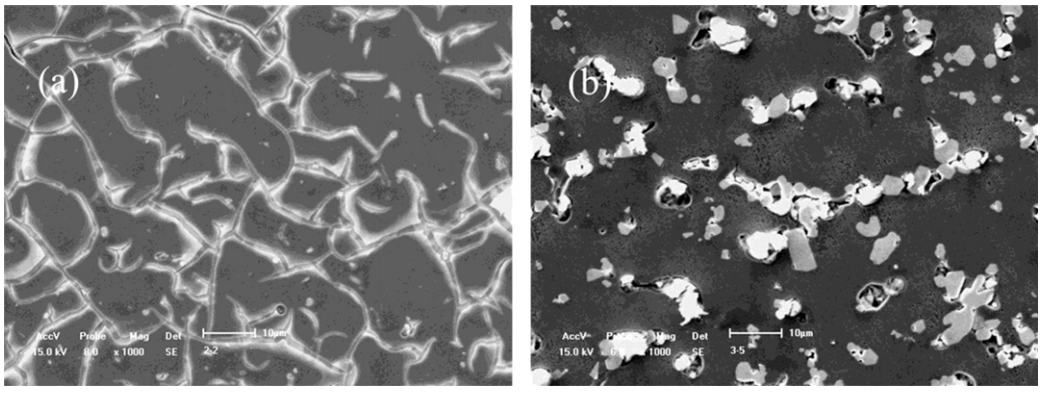

Fig. 6. SEM imagines of the $MlNi_{3.55}Co_{0.75-x}Mn_{0.4}Al_{0.3}(Cu_{0.75}P_{0.25})_x$ alloys after corrosion: (a) $x = 0$; (b) $x = 0.5$.

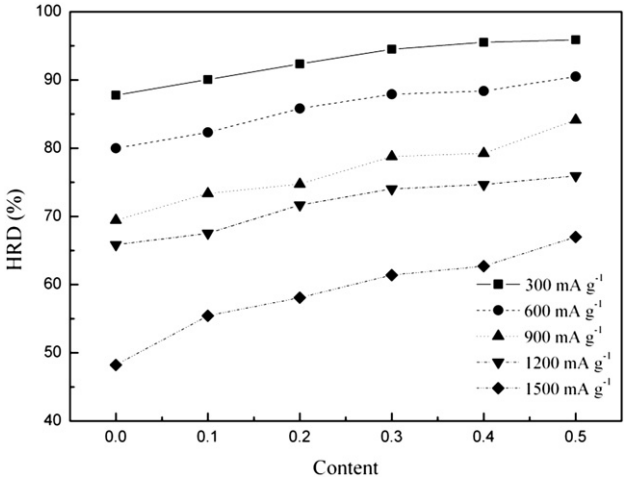

Fig. 7. High-rate discharge capacity of the $MlNi_{3.55}Co_{0.75-x}Mn_{0.4}Al_{0.3}(Cu_{0.75}P_{0.25})_x$ ($x = 0$–0.5) alloy electrodes.

is that the resistivity of Cu, Ni, Co is 1.69×10^{-8}, 6.84×10^{-8}, 6.64×10^{-8} Ω m respectively, and obviously Cu has lower electrical resistivity than others. Therefore, the addition of Cu enhances the effectiveness of the current collection processes, and further improves the charge-transfer process of the electrochemical reactions.

The hydrogen diffusion coefficient plays a dominant role within the electrode system, and is therefore still a research topic of great interest. The hydrogen diffusion behavior in hydrogen storage alloys is mainly studied by the constant potential method, whereas it can only be used to measure an average diffusion coefficient from the given depth of discharge (DOD) to fully discharge state (100% DOD), because this method ignores the fact that the hydrogen concentration changes in the measurement process [31]. Considering the variations of the hydrogen concentration in diffusion process, the GITT method is a more suitable instrument to research the diffusion behavior.

The GITT curves are shown in Fig. 9, and corresponding hydrogen diffusion coefficients shown to be dependent on the composition of the hydrogen storage alloys in Table 2.

$$\frac{dE}{d\sqrt{t}} = \frac{2V_m I_0}{nFS\sqrt{\pi D}}\left(\frac{dE}{dn}\right) \quad (2)$$

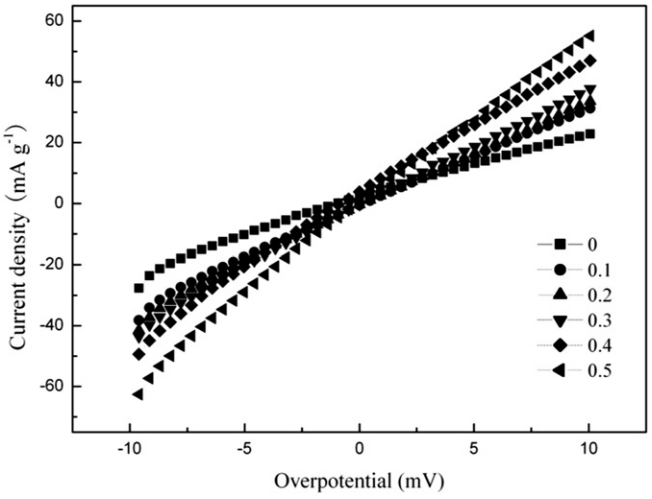

Fig. 8. Linear polarization curves of the $MlNi_{3.55}Co_{0.75-x}Mn_{0.4}Al_{0.3}(Cu_{0.75}P_{0.25})_x$ ($x = 0$–0.5) alloy electrodes.

Table 2
The charge-transfer resistance R_{ct}, the exchange current density I_0, the hydrogen diffusion coefficient D of the $MlNi_{3.55}Co_{0.75-x}Mn_{0.4}Al_{0.3}(Cu_{0.75}P_{0.25})_x$ ($x = 0$–0.5) alloy electrodes.

Content	R_{ct} (mΩ)	I_0 (mA g^{-1})	D (cm^2 s^{-1})
$x = 0$	421.9	61.88	4.72×10^{-11}
$x = 0.1$	298.1	87.58	7.99×10^{-11}
$x = 0.2$	278.2	93.82	1.41×10^{-10}
$x = 0.3$	251.9	103.6	1.88×10^{-10}
$x = 0.4$	211.9	123.2	2.29×10^{-10}
$x = 0.5$	173.4	150.5	2.98×10^{-10}

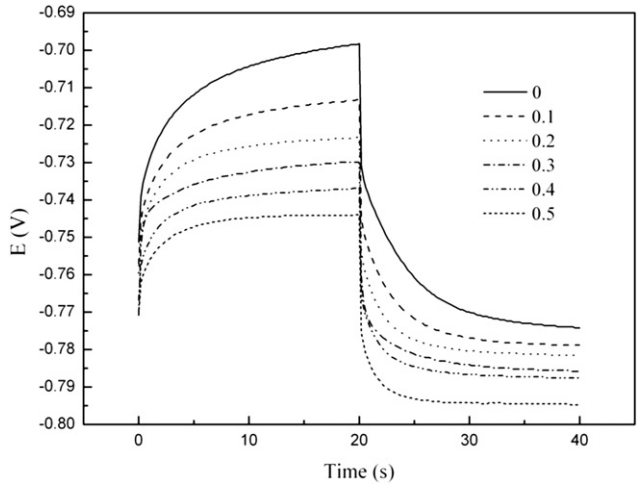

Fig. 9. GITT curves of the $MlNi_{3.55}Co_{0.75-x}Mn_{0.4}Al_{0.3}(Cu_{0.75}P_{0.25})_x$ ($x = 0$–0.5) alloy electrodes.

In the above equation [32], E is the voltage of the electrode (V), V_m is the mole volume of the alloys (cm^3 mol^{-1}), n is the number of transferred electrons in the electrode reaction, dE/dn is the slope of the coulometric titration curve.

It is found that the hydrogen diffusion coefficient increases from 4.72×10^{-11} cm^2 s^{-1} ($x = 0$) to 2.98×10^{-10} cm^2 s^{-1} ($x = 0.5$). The above results indicate that the hydrogen diffusion rate in the bulk alloy increases, which can be explained from following aspects.

The increase of the hydrogen diffusion coefficient with increasing Cu–P content is attributed to the fact that Cu has less affinity with hydrogen atoms than Co and Ni, which is in agreement with the investigations of Yukawa [33] and Nakatsuka [34]. On the other hand, the improvement of the hydrogen diffusion process is closely related to the multiple structures of the substitutional alloys. The fact that the alloy has excellent kinetics performance corresponds to the multiphase structures, since the phase boundary provides good tunnels for diffusion atoms [35–37].

We have studied the kinetics parameters of the Cu–P containing alloys by the electrochemical impedance spectroscopy method in our previous investigations. The obtained values of the exchange current density and the hydrogen diffusion coefficient increase with increasing Cu–P content, which is in agreement with the variations of the aforementioned results. However, there is a small discrepancy between the numeric values obtained by different electrochemical methods.

4. Conclusions

The effect of the substitution of Cu–P for Co on the microstructure and electrochemical performance of the $MlNi_{3.55}Co_{0.75-x}Mn_{0.4}Al_{0.3}(Cu_{0.75}P_{0.25})_x$ ($x = 0$–0.5) composite alloys are

investigated systematically. The conclusions can be summarized as follows:

(1) The results obtained by XRD, SEM and EDS indicate that the $MlNi_{3.55}Co_{0.75}Mn_{0.4}Al_{0.3}$ alloy consists of $LaNi_5$ phase, and the substitutional alloys are composed of multiphase structures, including the $LaNi_5$ phase, P-rich phase and Mn-rich phase. The abundance of the second phase increases with increasing Cu–P content.
(2) The electrochemical measurements show that the substitutional alloys can be easily activated to their maximum discharge capacity within only one cycle, but the maximum discharge capacity decreases from 296.8 mA h g^{-1} ($x = 0$) to 275 mA h g^{-1} ($x = 0.5$).
(3) With the increase of the Cu–P content, the capacity decay rate C_{100} initially decreases from 1.26 mA h g^{-1} $cycle^{-1}$ ($x = 0$) to 0.80 mA h g^{-1} $cycle^{-1}$ ($x = 0.3$), and then increases to 1.19 mA h g^{-1} $cycle^{-1}$ ($x = 0.5$), indicating that the substitution of Cu–P for Co has an advantageous effect on the cycle stability, but too much additives would deteriorate the cycle life endurance.
(4) The overall high-rate discharge capability is significantly improved with increasing Cu–P content. Especially at high discharge current density 1500 mA g^{-1}, the values of HRD increase from 48.23% to 67%. The linear polarization curves and GITT measurements reveal that the exchange current density increases from 61.88 mA g^{-1} ($x = 0$) to 150.5 mA g^{-1} ($x = 0.5$) and the hydrogen diffusion coefficient increases from 4.72×10^{-11} cm^2 s^{-1} ($x = 0$) to 2.98×10^{-10} cm^2 s^{-1} ($x = 0.5$), which are in agreement with the monotonous increase of the high-rate discharge capacity. The best compromise between excellent high-rate discharge capacity and favorable cycle stability of the series alloys is obtained when $x = 0.3$.

References

[1] S. Bliznakov, E. Lefterova, N. Dimitrov, K. Petrov, A. Popov, J. Power Sources 176 (2008) 381–386.
[2] K. Shinyama, Y. Magari, H. Akita, K. Kumagae, H. Nakamura, S. Matsuta, T. Nohma, M. Takee, K. Ishiwa, J. Power Sources 143 (2005) 265–269.
[3] Y.H. Xu, Y. Chen, J. Wu, D.C. Li, H. Ju, J.W. Zheng, Int. J. Hydrogen Energy 35 (2010) 6366–6380.
[4] S. Srivastava, R.K. Upadhyay, J. Power Sources 195 (2010) 2996–3001.
[5] L. Kong, B. Chen, K. Young, J. Koch, A. Chan, W. Li, J. Power Sources 213 (2012) 128–139.
[6] Z.H. Ma, J.F. Qiu, L.X. Chen, Y.Q. Lei, J. Power Sources 125 (2004) 267–272.
[7] X.Y. Zhao, Y. Ding, M. Yang, L.Q. Ma, Int. J. Hydrogen Energy 33 (2008) 81–86.
[8] M.V. Ananth, M. Raju, K. Manimaran, G. Balachandran, L.M. Nair, J. Power Sources 167 (2007) 228–233.
[9] E. Raekelboom, F. evas, B. Knosp, A. Percheron-Guégan, J. Power Sources 170 (2007) 520–526.
[10] P.H.L. Notten, R.E.F. Einerhand, J.L.C. Daams, J. Alloys Compd. 231 (1995) 604–610.
[11] D. Chartouni, F. Meli, A. Züttel, K. Gross, L. Schlapbach, J. Alloys Compd. 241 (1996) 160–166.
[12] J.M. Joubert, M. Latroche, R. Černý, A. Percheron-Guégan, K. Yvon, J. Alloys Compd. 330–332 (2002) 208–214.
[13] C. Iwakura, K. Fukuda, H. Senoh, H. Inoue, M. Matsuoka, Y. Yamamoto, Electrochim. Acta 43 (1998) 2041–2046.
[14] H.G. Pan, J.X. Ma, C.S. Wang, C.P. Chen, Q.D. Wang, Electrochim. Acta 44 (1999) 3977–3987.
[15] B. Zhang, W.Y. Wu, X. Bian, G.F. Tu, J. Alloys Compd. 538 (2012) 189–192.
[16] K.Y. Shu, S.K. Zhang, Y.Q. Lei, G.L. Lü, Q.D. Wang, Int. J. Hydrogen Energy 28 (2003) 1101–1105.
[17] W.K. Hu, H. Lee, D.M. Kim, S.W. Jeon, J.Y. Lee, J. Alloys Compd. 268 (1998) 261–265.
[18] Y.H. Zhang, G.Q. Wang, X.P. Dong, S.H. Guo, J.Y. Ren, X.L. Wang, J. Power Sources 148 (2005) 105–111.
[19] Y.H. Zhang, M.Y. Chen, X.L. Wang, G.Q. Wang, Y.F. Lin, Y. Qi, J. Power Sources 125 (2004) 273–279.
[20] Y. Nakamura, R.C. Bowman, E. Akiba, J. Alloys Compd. 373 (2004) 183–193.
[21] W.Z. Tang, Y.X. Gai, H.Y. Zheng, J. Alloys Compd. 224 (1995) 292–298.
[22] A. Percheron-Guégan, C. Lartigue, J.C. Achard, J. Less-Common Met. 109 (1985) 287–309.
[23] P.H.L. Notten, R.E.F. Einerhand, J.L.C. Daams, J. Alloys Compd. 210 (1994) 221–232.
[24] P.H.L. Notten, J.L.C. Daams, R.E.F. Einerhand, J. Alloys Compd. 210 (1994) 233–241.
[25] M. Tliha, H. Mathlouthi, C. Khaldi, J. Lamloumi, A. Percheron-Guégan, J. Power Sources 160 (2006) 1391–1394.
[26] F. Feng, D.O. Northwood, J. Power Sources 136 (2004) 346–350.
[27] D. Barsellini, A. Visintin, W.E. Triaca, M.P. Soriaga, J. Power Sources 124 (2003) 309–313.
[28] J. Liu, Y.F. Yang, P. Yu, Y. Li, H.X. Shao, J. Power Sources 161 (2006) 1435–1442.
[29] M. Raju, M.V. Ananth, L. Vijayaraghavan, J. Power Sources 180 (2008) 830–835.
[30] P.H.L. Notten, P. Hokkeling, J. Electrochem. Soc. 138 (1991) 1877–1885.
[31] X.X. Yuan, Z.F. Ma, Y.N. Nuli, N.X. Xu, J. Alloys Compd. 385 (2004) 90–95.
[32] W. Weppner, R.A. Huggins, J. Electrochem. Soc. 124 (1977) 1569–1578.
[33] H. Yukawa, M. Moringa, Y. Takahashi, J. Alloys Compd. 253–254 (1997) 322–325.
[34] K. Nakatsuka, M. Yoshino, H. Yukawa, M. Morinaga, J. Alloys Compd. 293–295 (1999) 222–226.
[35] R. Tang, L.Q. Liu, Y.N. Liu, G. Yu, Int. J. Hydrogen Energy 28 (2003) 815–819.
[36] Y.H. Zhang, G.Q. Wang, X.P. Dong, S.H. Guo, J.M. Wu, X.L. Wang, J. Alloys Compd. 379 (2004) 298–304.
[37] H. Ye, H. Zhang, W.Q. Wu, T.S. Huang, J. Alloys Compd. 312 (2000) 68–76.